Korean J. Chem. Eng., **20**(3), 560-565 (2003)

An Electrochemical Study of Cathodic Protection of Steel Used for Marine Structures

Seong-Jong Kim†, Masazumi Okido and Kyung-Man Moon*

Graduate School of Engineering, Nagoya University, Furo-cho, Chikusa-ku, Nagoya 464-8603, Japan
*Korea Maritime University, Busan 606-791, Korea
(*Received 18 June 2002 • accepted 9 May 2003*)

Abstract−Impressed current cathodic protection can result in hydrogen embrittlement, which can cause trouble with high-strength steels, particularly at welds. Therefore, the limiting potential for hydrogen embrittlement should be examined in detail as a function of the cathodic protection potential. This study investigated the effects of post-weld heat treatment (PWHT) on marine structural steels from an electrochemical viewpoint. In addition, the slow strain rate test (SSRT) was used to investigate both the electrochemical and mechanical effects of PWHT on impressed current cathodic protection. According to the SSRT, the optimum cathodic protection potential was −770 mV [with a saturated calomel electrode (SCE)]. SEM fractography analysis showed that the fracture morphology at an applied cathodic protection potential of −770~−850 mV (SCE) was a dimpled pattern with ductile fractures, while a transgranular pattern was seen at potentials below −875 mV (SCE). Therefore, the cathodic protection potential range should be −770~−850 mV (SCE).

Key words: Slow Strain Rate Test, Impressed Current Cathodic Protection, Hydrogen Embrittlement, Post-weld Heat Treatment

INTRODUCTION

Offshore structures, such as marine airports, bridges, marine platforms, undersea tunnels, and vessels are getting much larger, leading to important economic considerations of maintenance and repair of such structures. Offshore structures are exposed to the harsh marine environment, including the effects of waves, sand, storms, and tides. Therefore, these structures need to be protected against corrosion. Cathodic protection is widely used for marine structural steel. However, over-protection during impressed current cathodic protection results in hydrogen embrittlement of the high-strength steel that is used in marine structures.

Most failures of marine structures are likely associated with the corrosion of welded parts and hydrogen embrittlement resulting from cathodic protection [Rothwell and Turner, 1990; Singh Raman and Granmoorthy, 1995; Hashimoto, 1998]. The corrosion problem might be due to physical and metallurgical parameters [Masazi, 1964]. A galvanic cell results from the potential difference between each welded part. Post-weld heat treatment (PWHT) is often used to reduce galvanic corrosion on welded parts [Bhaduri et al., 1995; Bloch et al., 1997]. The correlation between the mechanical properties of steel and hydrogen embrittlement has been investigated in notched base metal (BM) parts by using the slow strain rate test (SSRT). The SSRT as a function of cathodic potential has been examined closely at the limiting potential not causing hydrogen embrittlement and at the optimum cathodic protection potential [Kim and Wilde, 1979; Lee et al., 1985; Saito et al., 1987]. Therefore, the results of this study should serve as a good reference, not only for preventing hydrogen embrittlement, but also for determining the mechanical properties of the BM used in the construction of marine structures and vessels.

†To whom correspondence should be addressed.
E-mail: kmue43aksj@hanmail.net

EXPERIMENTAL

1. Test Specimens and PWHT

High-strength steel was used for SSRT and PWHT test specimens. Each test specimen was 358×4×23.6 mm (long×wide×thick), with a gauge length of 59 mm. The test specimens were made according to section No. 14B of JIS Z2201. A piece was welded to the center of the test specimen. The groove angle of the welded part was 35±5°, and 0.5×4.8 notches (wide×deep) were made on both sides of the BM to produce fractures in the BM.

Table 1 shows the chemical composition and mechanical properties of the high-strength steel and chemical composition of the filler metal. Flux-cored arc-welding (FCAW) was used and the welding conditions are detailed in Table 2. For PWHT, the specimens were heated at 80 °C per hour to 550, 600, or 650 °C, kept at that temperature for 1.5 hours, and then furnace cooled. It is commonly re-

Table 1. Chemical compositions and mechanical properties of used steel specimens and chemical compositions of filler metals

(a) Chemical compositions of used steel (%)

C	Si	Mn	P	S	Fe
0.17	0.45	1.26	<0.0027	<0.0008	Balance

(b) Mechanical properties of used steel

T.S(MPa)	Y.S(MPa)	Elongation(%)
597	360	26.6

(c) Chemical compositions of filler metals (%)

C	Si	Mn	P	S	Ni
0.04	0.40	1.20	0.012	0.008	1.50

Table 2. Welding parameters in FCAW

Pass no.	Welding process	Shielding gas	Filler metals		Type & polarity	Current (A)	Voltage (V)	Travel speed (cm/min)
			AWS class	Dia. (mm)				
1						180-240	23-29	10-20
2	FCAW	CO_2	E80T1-K2	1.2	DCRP	220-280	25-32	20-30
3-8						250-300	28-32	20-40

ported that the optimum PWHT temperature range of high-strength steel is from 550 to 650 ℃.

2. Experimental Method

2-1. Electrochemical Test

The BM surface area of the test specimen used to measure the cathodic and anodic polarization trend and corrosion current density was 6.45 cm^2, including the heat-affected zone (HAZ) and welded metal (WM) part. This area was polished with successively finer emery paper to No. 600 grit.

The surface area used to measure the cathodic polarization curves was 1 cm^2. The curves were measured at a scan rate of 1 mV/sec using a saturated calomel electrode (SCE) as the reference electrode and a Pt counter electrode.

In addition, 6.5 cm^2 of the welded parts were exposed in natural seawater (volume: 1 liter) and protected by a sacrificial Al anode (exposed area: 0.123 cm^2). The flow was varied with a stirrer and magnetic ball. The weight loss of the sacrificial anode after immersion for 7 days was determined. The chemical composition of the Al alloy sacrificial anode is shown in Table 3.

2-2. Slow Strain Rate Test

SSRT specimens were exposed to natural seawater. The specimens were fitted with a jig for an Instron machine. The seawater in the cell was circulated continuously from the upper to the lower tank with a pump. The SSRT was carried out at a strain rate of 3×10^{-7}/sec when a constant potential was maintained with a potentiostat and function generator. The properties of the seawater used are given in Table 4.

RESULTS AND DISCUSSION

1. Electrochemical Test

Fig. 1 compares the BM microstructure of as-welded steel and specimens subjected to the PWHT at various temperatures. As shown in Photo 1, perlite and ferrite microstructures were seen in all the specimens. The perlite band appeared to disappear as a result of diffusion with increasing PWHT temperature. In the cathodic and anodic polarization curves as a function of the PWHT temperature of the welded joint, the activation reaction due to the dissolution of Fe ($Fe\rightarrow Fe^{+2}+2e^-$) occurred in the anodic polarization curves, while concentration polarization due to the reduction of dissolved oxygen ($O_2+2H_2O+4e\rightarrow 4OH^-$) appeared in the cathodic polarization curves.

We calculated the corrosion current density using the Stern-Geary formula and the diffusion-limiting current density in the anodic and cathodic polarization curves. The Stern-Geary formula is

$$i_{corr}=\frac{1}{2.3}\frac{i_{(applied)}}{\Delta\phi}\left(\frac{\beta_c\beta_a}{\beta_c+\beta_a}\right) \quad (1)$$

Where, $i_{(applied)}$ is the applied current density, $\Delta\phi$ is the polarization potential value, and β_c and β_a are the Tafel slopes of the cathodic and anodic reactions, respectively. Formula (1) is used for both the anodic and cathodic Tafel slopes. By contrast, for the anodic Tafel slope, the diffusion-limiting current density is regarded as the corrosion current density for corrosion caused by the reduction of oxygen dissolved in natural seawater. In this case, the cathodic Tafel slope becomes infinity, so the formula becomes

$$i_{corr}=\frac{\beta_a}{2.3}\frac{i_{(applied)}}{\Delta\phi} \quad (2)$$

Variation in i_{corr} as a function of the applied Tafel coefficient according to the PWHT conditions is shown in Fig. 2. The corrosion current densities for as-welded specimens were greater than those

Table 3. Chemical compositions of Al alloy sacrificial anode

Composition	Fe	Si	Cu	Zn	In	Al
Weight percent (%)	0.084	0.0375	0.0325	5.24	0.0175	Balance

Table 4. Qualities of sea water solution used in SSRT experiment

Temperature	Specific resistance	pH	Chloride	Dissolved oxygen	Redox potential
23 ℃	21.46 Ωcm	8.0	16,197 ppm	7.7 ppm	+210 mV

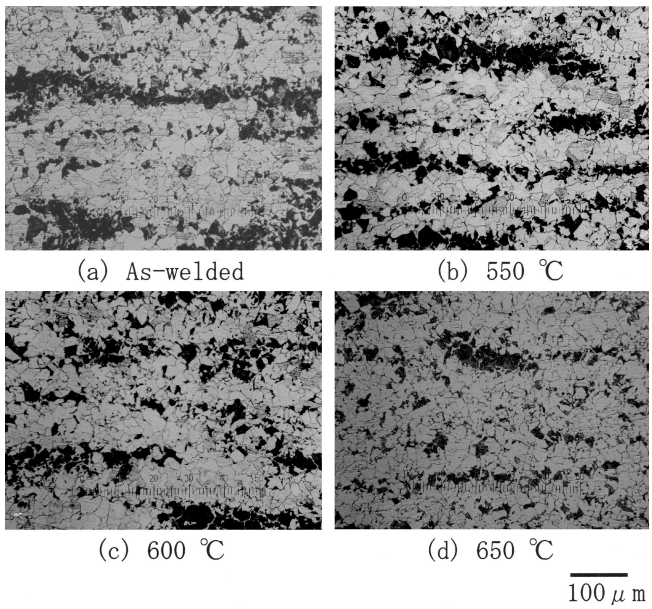

Fig. 1. Variation of BM microstructures in the case of as-welded and various PWHT temperature.

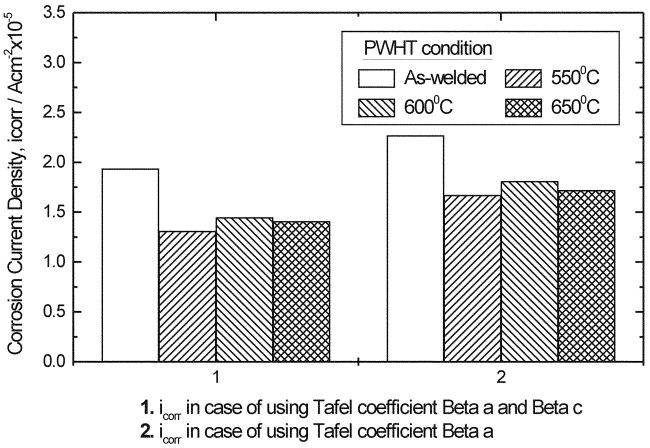

Fig. 2. Variation of i_{corr} as a function of applied Tafel coefficient in the case of PWHT condition.

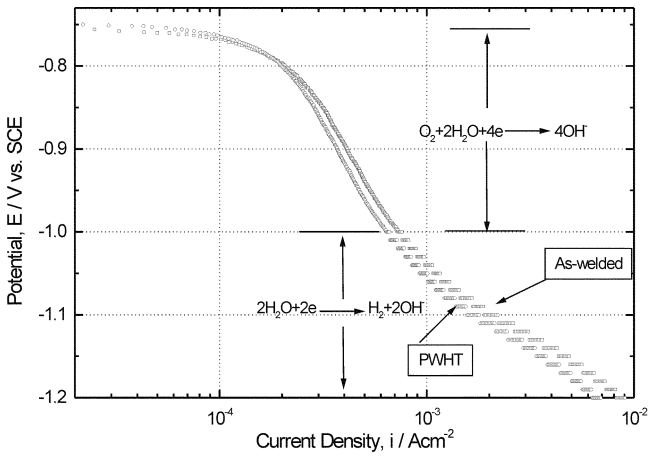

Fig. 4. Cathodic polarization curves of welding metal of in natural sea water solution.

of PWHT specimens, regardless of whether formula (1) or (2) was used. The smallest corrosion current density was seen in PWHT specimens treated at 550 °C. Moreover, the corrosion current density using formula (1) was smaller than that using formula (2).

For cathodic protection using Al alloy, the ratio of the area of the cathode (including BM, WM, and HAZ) to the Al anode was 52 (cathode: 6.45 cm^2) to 1 (Al anode: 0.123 cm^2). The current generated by the sacrificial Al anode was greater in the as-welded specimen than with PWHT. The lowest anodic-generating current was observed in PWHT specimens treated at 550 °C. Therefore, the smaller the anodic generating current, the smaller the anodic weight loss. The anodic generating current at a flow rate of 3 cm/sec is generally higher than in the static condition.

Fig. 3 shows the relationship between the Al anode weight loss and the PWHT conditions at flow rates of 0 and 3 cm/sec. The anodic current generated at 3 cm/sec was larger than that at 0 cm/sec, and the anode weight loss was greater. This was thought to be due to the relative increase in the movement of seawater with increasing flow rate. In other words, the potential difference between the Al alloy and cathode increases with the decrease in the concentration polarization due to the reduction of dissolved oxygen. The anodic current generated and the anode weight loss were both larger at 3 cm/sec than in the static condition. The lowest weight loss from the Al anode was in the 550 °C PWHT specimen.

The optimum PWHT temperature with the electrochemical method was 550 °C. Accordingly, we used only as-welded and 550 °C PWHT specimens in the SSRT.

2. Evaluating Mechanical Properties by the SSRT

The notched BM parts of as-welded and PWHT specimens were subjected to the SSRT as a function of cathodic potential.

Fig. 4 shows the cathodic polarization curves of BM in natural seawater. The two cathodic polarization curves in Fig. 4 appear similar, but the corrosion potential of the 550 °C PWHT specimen is similar to that of the as-welded specimen. There is no clear difference in the polarization curves in the region between the open circuit potential and −800 mV. By contrast, the current density in the PWHT specimen is smaller than that in the as-welded specimen at below −800 mV. The turning point between concentration polarization due to the reduction of dissolved oxygen and activation polarization due to hydrogen gas generation ($2H_2O+2e^- \rightarrow H_2+2OH^-$) was approximately −1,000 mV, regardless of whether as-welded or PWHT specimens were used. However, the potential limiting hydrogen embrit-

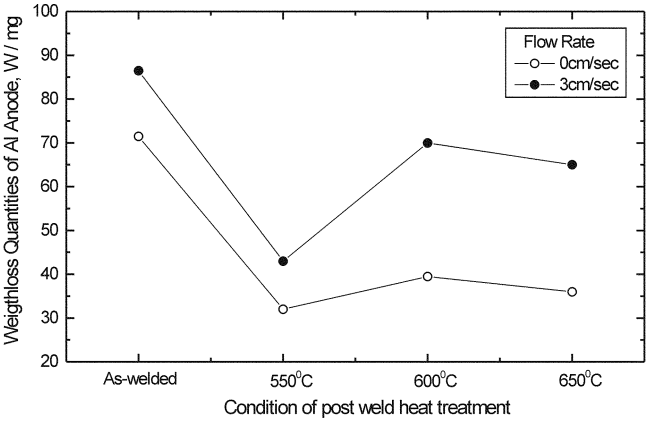

Fig. 3. Relationship between Al anode weight loss quantity and PWHT conditions in the case of flow rate 0 cm/sec, 3 cm/sec.

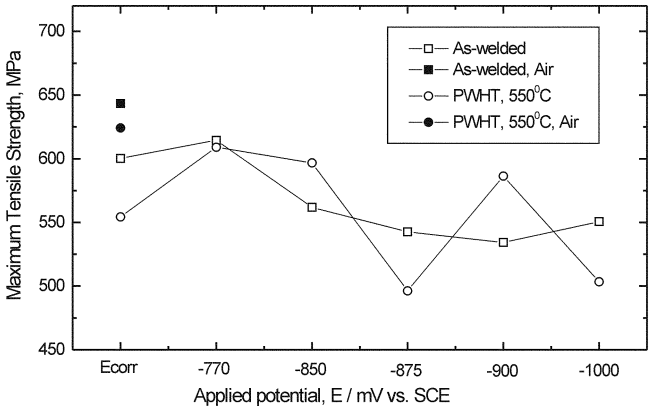

Fig. 5. Relationship between maximum tensile strength and applied cathodic potential in as-welded and post-weld heat treated specimen.

tlement cannot be decided only from the cathodic polarization curves. Therefore, we performed the SSRT at a constant cathodic potential in order to investigate the potential limiting hydrogen embrittlement.

Fig. 5 shows the relationship between the maximum tensile strength and constant cathodic potential in as-welded and PWHT specimens. The greatest maximum tensile strength in as-welded and PWHT specimens was observed in air at 643.4 and 624.2 MPa, respectively. Moreover, the tensile strength was highest at a cathodic potential of −770 mV for both the as-welded and PWHT specimens. There were no correlations between yield strength, stress at final failure, and constant cathodic potential, neither for the as-welded nor the PWHT conditions.

The relationship between elongation and constant cathodic potential in the as-welded and PWHT conditions is shown in Fig. 6. Elongation is decreased by shifting to a negative cathodic potential, which readily results in the evolution of hydrogen. However, the elongation values for 550 °C PWHT specimens are generally greater than for as-welded specimens throughout the range of potentials. This suggests that hydrogen embrittlement readily occurs with gradually increasing negative potential.

Fig. 7 shows the relationship between time-to-fracture and constant cathodic potential. The time-to-fracture was greatest when the

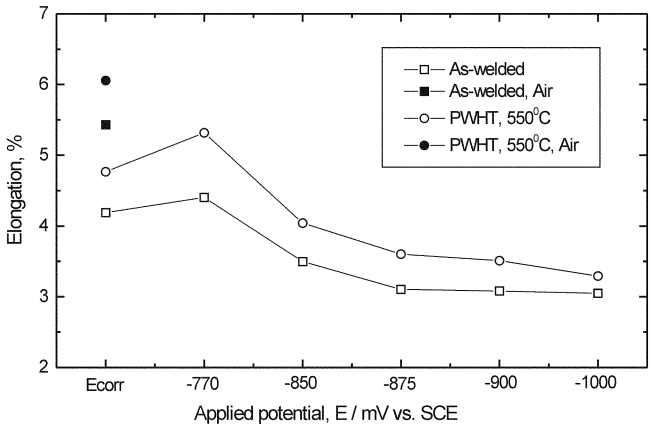

Fig. 6. Relationship between elongation and applied cathodic potential in as-welded and post-weld heat treated specimen.

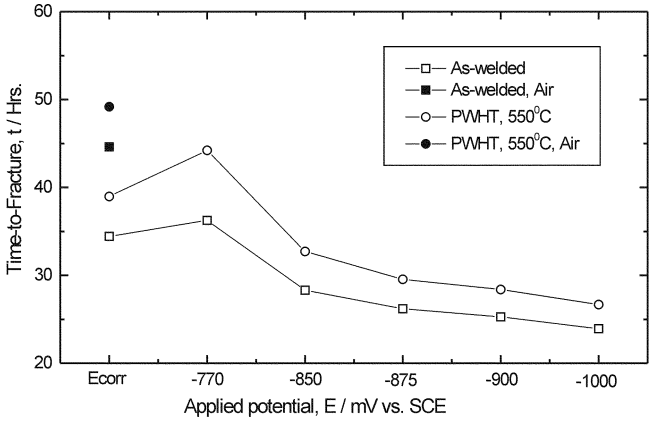

Fig. 7. Relationship between time-to-fracture and applied cathodic potential in as-welded and post-weld heat treated specimen.

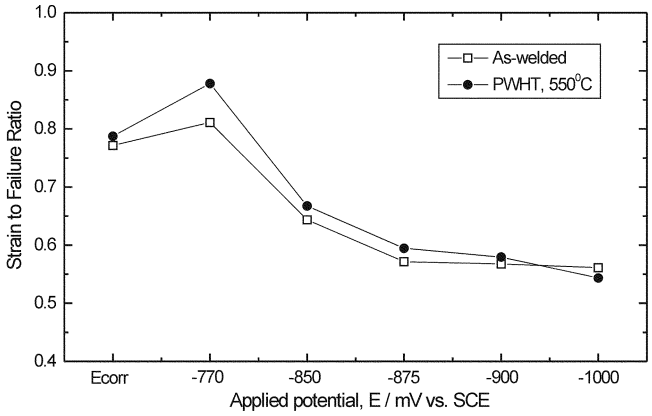

Fig. 8. Relationship between strain to failure ratio and applied cathodic potential in as-welded and post-weld heat treated specimen.

cathodic potential was −770 mV, regardless of PWHT condition. The time-to-fracture decreased as the cathodic potential became more negative, possibly due to the influence of hydrogen embrittlement.

The relationship between the strain-to-failure ratio and the cathodic potential is shown in Fig. 8. The strain-to-failure ratio is the ratio of the percent elongation in seawater to that in air. This suggests that hydrogen embrittlement decreases with increasing hydrogen embrittlement ratio (strain-to-failure ratio). The hydrogen embrittlement ratios in the as-welded and PWHT conditions were greatest at −770 mV compared with other potentials. Overall, the hydrogen embrittlement ratio was greater for PWHT versus as-welded specimens.

The results of the SSRT as a function of cathodic potential suggest that there is no correlation between maximum tensile strength and hydrogen embrittlement. Conversely, there were correlations between elongation, time-to-fracture, the strain-to-failure ratio, and hydrogen embrittlement. The optimum cathodic protection potential for as-welded and PWHT specimens was −770 mV, because the elongation, time-to-fracture, and strain-to-failure ratio were greatest at −770 mV for all the cathodic potentials applied. The polarization curves (Fig. 4) were largely divided into oxygen reduction and hydrogen ion reduction portions. The current density increased as the cathodic potential declined. With a high current density, hydrogen ion reduction was more prominent than the oxygen reduction reaction. In general, the protection potentials of plain carbon and low-alloy steels are below −770 mV (SCE) in natural seawater [Von Baeckmann et al., 1997]. The lowest current density was observed at a cathodic protection potential of about −770 mV. Therefore, the elongation and time-to-fracture are maximal at a potential of −770 mV [Kim et al., 2001]. According to Yamaguchi et al. [1998] and Maier and Kaesche [1990], the hydrogen input activity increases with increasing negative potential or with increasing current density up to a certain level before reaching a plateau.

The mechanical properties of high-strength steel were investigated at a constant cathodic potential by using the SSRT. The results indicate that susceptibility to hydrogen embrittlement results from the evolution of hydrogen with increasing negative cathodic potential. However, these investigations were qualitative rather than quan-

titative. It would be beneficial if hydrogen embrittlement could be estimated quantitatively.

3. Fractography Analysis

Fig. 9 and 10 are SEM fractographies of the fractured surface as a function of cathodic potential using the SSRT method. As shown in Fig. 10, only dimples were seen in air, E_{corr}, at potentials of –770 and −850 mV in both the as-welded and PWHT conditions, while the fractographies at potentials below −875 mV show a mixture of dimple and quasi cleavage (QC) in both the as-welded and PWHT conditions. This mixed phenomenon, with few dimples and QC, was seen at potentials of −875, −900, and −1,000 mV. The fracture mode at −1,000 mV included considerable QC, especially in the as-welded specimens, in the range of hydrogen embrittlement [de Kazinczy, 1954; Thompson and Chesnutt, 1979; Francis et al., 1999]. These results suggest that the susceptibility to hydrogen embrittlement decreases markedly with increasing elongation, time-to-fracture, strain-to-failure ratio, and amount of dimpling with PWHT. Conversely, although a cathodic potential of –875 mV is within the range of concentration polarization due to the reduction of dissolved oxygen, some influence of hydrogen embrittlement was seen in both the as-welded and PWHT conditions. It is thought that this was caused by atomic hydrogen (H) generated in the reaction $H^+ + e^- \rightarrow H$. Atomic hydrogen gas is generated at decreasing pH due to the hydrolysis reaction ($FeCl_2 + 2H_2O \rightarrow Fe(OH)_2 + 2HCl$). This atomic hydrogen gas can penetrate the interior of metal [Beahem, 1972; Bandyyopadhy et al., 1983]. Consequently, notched specimens are fractured by atomic hydrogen gas in the region of the oxygen reduction reaction. There were many more shear lips in PWHT specimens compared to as-welded specimens. This suggests that elongation, time-to-fracture, and strain-to-failure ratio increase with increasing shear lip in PWHT. Thus, it is suggested that the optimum cathodic protection potential range that does not cause hydrogen embrittlement is from 770 to −850 mV in both the as-welded and PWHT conditions.

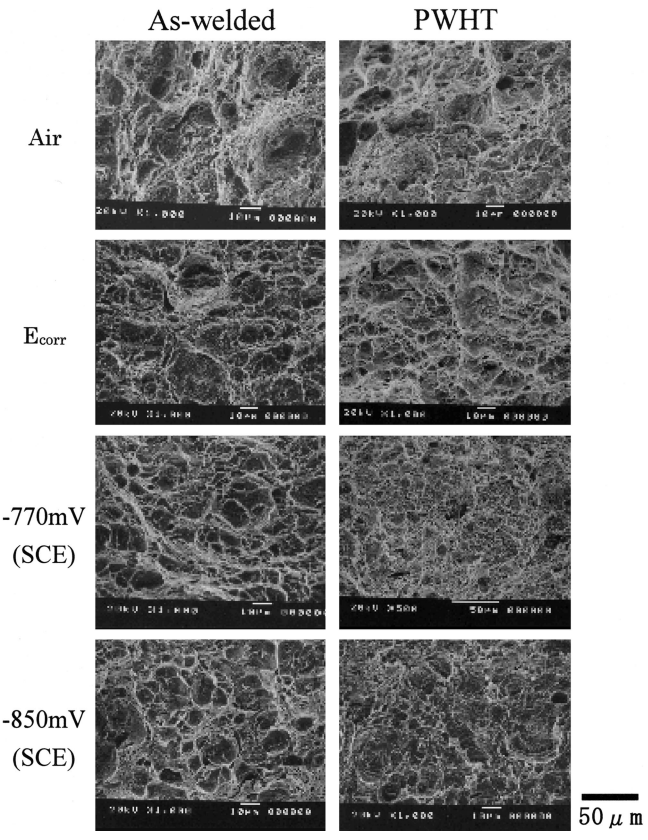

Fig. 9. Fractography at Air, E_{corr}, and applied potential –770 mV, –850 mV.

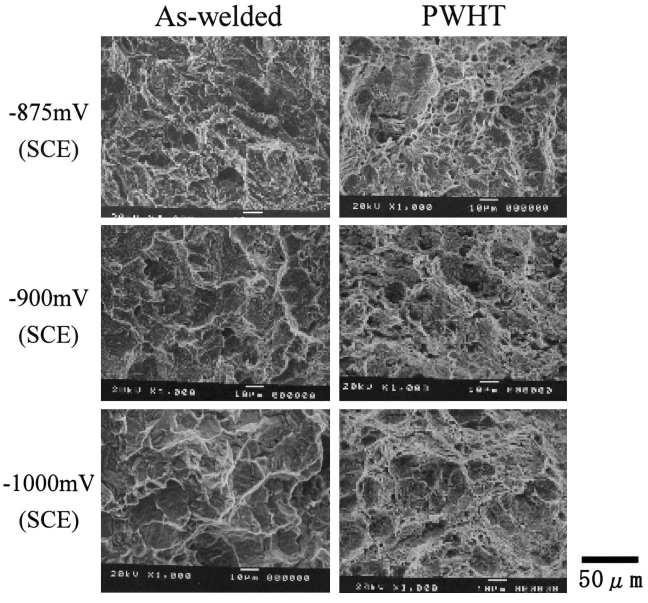

Fig. 10. Fractorgraphy at applied potential –875 mV, –900 mV and –1,000 mV.

CONCLUSIONS

PWHT increased corrosion resistance. It also decreased the current generated by the aluminum anode, and anode weight loss when high-strength steel was cathodically protected by an Al anode. There did not appear to be any correlation between maximum tensile strength and hydrogen embrittlement. However, the elongation, time-to-fracture, and strain-to-failure ratio decreased as the potential was lowered due to hydrogen evolution. The QC fracture mode was also observed at lower potentials. The susceptibility to hydrogen embrittlement increased significantly with decreasing elongation and time-to-fracture as a result of a shift to lower potential. The susceptibility to hydrogen embrittlement with PWHT also decreased with increasing elongation, time-to-fracture, and a large amount of dimpling. In the SEM fractography analysis, the fracture morphology at applied cathodic potentials between –770 and –850 mV showed a dimple pattern with ductile fractures, which changed to a transgranular pattern at potentials under −875 mV.

Consequently, the optimum cathodic protection potential range, not causing hydrogen embrittlement, is between −770 and −850 mV (SCE) with PWHT at 550 °C and in the as-welded condition.

REFERENCES

Bandyyopadhy, N., Kameda, J. and McMahon, C. J. Jr., "Hydrogen-induced Cracking in 4340-type Steel: Effects of Composition, Yield Strength, and H_2 Pressure," *Metallurgical Transactions*, **14A**, 881

(1983).
Beahem, C. D., "A New Model for Hydrogen-assisted Cracking (Hydrogen Embrittlement)," *Metallurgical Transactions*, **3**, 437 (1972).
Bhaduri, A. K., Sujith, S., Srinivasan, G., Gill, T. P. S. and Mannan, S. L., "Optimized PWHT Procedures for 17-4 PH Stainless Steels," Welding Research Supplement, 153 (1995).
Bloch, C., Hill, J. and Connell, D., "Proper PWHT Can Stop Stress-induced Corrosion," *Welding Journal*, **May**, 31 (1997).
de Kazinczy, F., "A Theory of Hydrogen Embrittlement," *Journal of Iron and Steel Institute*, **177**, 85 (1954).
Francis, R., Byrne, G. and Warbartan, G. R., "The Effect of Cathodic Protection on Duplex Stainless Steels in Sea Water," An Official NACE International Publication, 46 (1999).
Hasimoto, T., "Effect of Welding on Corrosion of Chemical Plants," *Boshoku Gijutsu*, **37**, 559 (1988).
Kim, C. D. and Wilde, B. E., "A Review of the Constant Strain Rate Stress Corrosion Cracking," *ASTM STP*, **665**, 97 (1979).
Kim, S. J., Park, T. W., Shim, I. O., Kim, J. H., Kim, Y. S. and Moon, K. M., "A Study of Hydrogen Embrittlement Limit Potential of Cu-containing High Strength Low Alloy Steel for Marine Structure by Potentiostatic SSRT Method," *Journal of the Korea Welding Society*, **19**, 45 (2001).
Lee, K. H., Cragnolino, G. and Macdonald, D. D., "Effect of Heat Treatment Applied Potential on the Caustic Stress Corrosion Cracking of Inconel 600," *Corrosion*, **41**, 540 (1985).
Maier, H. J. and Kaesche, H., "Hydrogen Effects on Material Behavior," Japan High Pressure Technology Association, Stress Annealing Committee Section, 3 (1982).
Masazi, O., "On Anti-corrosion Property of Steel's Weldments," *Boshoku Gijutsu*, **13**, 7 (1964).
Moody, N. R. and Thompson, A. W., "TMS," Warrendale, PA, 733 (1990).
Rothwell, N. and Turner, M. E. D., "Corrosion Problems Associated with Weldments," *Materials Performance*, **Feb**., 55 (1990).
Saito, M., Shoji, T., Takahasi, H., Miura, K. and Kumabu, M., "Evaluation of SCC of High Strength Steel by SSRT Method Under Marine Environments," *Journal of the Japan Mechanical Society(A)*, **54**, 746 (1987).
Singh Raman, R. K. and Granmoorthy, J. B., "Oxidation Behavior of Weld Metal, HAZ and Base Metal Regions in Weldments of Cr-Mo Steels," *Welding Research Supplement*, **Apr**., 133 (1995).
Thompson, A. W. and Chesnutt, J. C., "Identification of a Fracture. Mode: The Tearing Topography Surface," *Metallurgical Transactions*, **10A**, 1193 (1979).
Von Baeckmann, W., Schwenk, W. and Prinz, W., "Handbook of Cathodic Corrosion Protection," Gulf Publishing Company, Houston, 72 and 369 (1997).
Yamaguchi, Y., Nonaka, H. and Yamakawa, K., *Corrosion*, **53**, 147 (1998).